Journal of Inorganic Biochemistry 175 (2017) 118–128

Contents lists available at ScienceDirect

Journal of Inorganic Biochemistry

journal homepage: www.elsevier.com/locate/jinorgbio

Effect of tunable redox behavior of bis chelate substituted 1, 10-phenantroline Cu(II) complexes on its reaction with superoxide anion in DMSO. Toward a simple criterion to identify a SOD-like mechanism

Mayra E. Manzanera-Estrada[a], Marisela Cruz-Ramírez[a], Marcos Flores-Alamo[b], José Miguel Gracia y Jiménez[c], Rodrigo Galindo-Murillo[d], Juan Carlos García-Ramos[e,1], Lena Ruiz-Azuara[b], Luis Ortiz-Frade[a,*]

[a] Centro de Investigación y Desarrollo Tecnológico en Electroquímica, Pedro Escobedo, Querétaro 76703, Mexico
[b] Facultad de Química, Universidad Nacional Autónoma de México, Coyoacán, 04510 DF, Mexico
[c] Instituto de Física, Benemérita Universidad Autónoma de Puebla, Apdo. Postal J-48, Puebla, Pue. 72570, Mexico
[d] Department of Medicinal Chemistry, College of Pharmacy, University of Utah, 2000 East 30 South Skaggs 201, Salt Lake City, UT 84112, United States
[e] Departamento de Fisicoquímica, Instituto de Química, Universidad Nacional Autónoma de México, Coyoacán, 04510, Ciudad de México, Mexico. Currently at Centro de Nanociencia y Nanotecnología, UNAM.

ARTICLE INFO

Keywords:
Copper (II)-1,10-phenantroline complexes
Biomimetic metal complexes
SOD-like mechanism
Electrochemistry

ABSTRACT

In this work we report a series of Cu(II) complexes $[Cu(N\text{-}N)_2(X)]^+$, (N-N = substituted 1,10-phenanthroline derivatives and $X = Cl^-$ or NO_3^-), with tunable $E_{1/2}$ for electrochemical reduction $[Cu^{II}(N\text{-}N)_2(X)]^+ + 1e^- \rightleftharpoons [Cu^{I}(N\text{-}N)_2] + X^-$. The disproportion of $O_2^{\bullet -}$ was explored in presence of the electro-generated species $[Cu^{I}(N\text{-}N)_2]^+$ using cyclic voltammetry in a non-aqueous media, arising a new simple method to propose a SOD-like mechanism, which can be used as a quick guide test for a compound, before being proven in biological assays. It was found that complexes with high negative half wave potential values ($E_{1/2}$) for Cu(II)/Cu (I) couple shown a current increment for oxygen reduction, related to the capability of the disproportion of this reactive oxygen species.

1. Introduction

Intracellular superoxide dismutase enzyme (SOD), has the role to protect the cell against the superoxide radical ($O_2^{\bullet -}$) generated in the mitochondria during the cellular respiration [1]. This family of enzymes present different metallic centers in the active site, such as Cu (II)/Zn(II), Fe(III), Mn(III) or Ni(III), with homologies in the amino acid sequence in the protein domain. In particular, the most studied and well known system is Cu/Zn-SOD, where Cu(II) and Zn(II) are coordinated to aromatic nitrogen atoms from histidine residues [1,2]. A remarkable difference between normal and cancer cells is the low amount and the decreased activity of Mn-SOD and Zn/Cu-SOD enzymes [3–5]. This fact has motivated the use of Zn/Cu-SOD for the treatment of solid tumors in mice [6]. However, the use of this enzyme in medical treatments is limited due its low capacity to pass through membrane cell, change in activity by pH or temperature, and its high cost of production and purification. The above-mentioned has attracted the attention to design new copper-SOD biomimetic compounds [7–13]. The reaction mechanism of a Cu/Zn-SOD or a Cu(II) biomimetic system consists in the disproportion of superoxide radical in three steps. The first one is the interaction between the active site and the radical $O_2^{\bullet -}$, followed by the second step where molecular oxygen (O_2) is generated. In the third step the formation of hydrogen peroxide (H_2O_2) is proposed, see reactions (1)–(3) [14,15].

$$[Cu^{II}L] + O_2^{\cdot -} \rightarrow [Cu^{II}L \cdot\cdot O_2^{\cdot -}] \quad (1)$$

$$[Cu^{II}L\ O_2^{\cdot -}] \rightarrow [Cu^{I}L] + O_2 \quad (2)$$

$$[Cu^{I}L] + O_2^{\cdot -} + 2H^+ \rightarrow [Cu^{II}L] + H_2O_2 \quad (3)$$

It is a necessary condition in a SOD, and in a biomimetic compound, the existence of variable oxidation states in the metal center, with the low reorganization energy. Therefore, the homogeneous electron transfer between the oxidized or reduced form of the active site with $O_2^{\bullet -}$ (reactions (2) and (3)) should be fast. In the case of the biomimetic systems, it has been proposed that the redox potential value of the

* Corresponding author.
E-mail address: lortiz@cideteq.mx (L. Ortiz-Frade).
[1] Currently at Centro de Nanociencia y Nanotecnología, UNAM, Mexico.

http://dx.doi.org/10.1016/j.jinorgbio.2017.07.013
Received 23 February 2017; Received in revised form 10 July 2017; Accepted 13 July 2017
Available online 18 July 2017
0162-0134/

couple Cu(II)L/Cu(I)L should lie in a range from − 330 mV (vs. NHE at pH 7; $O_2/O_2^{\bullet -}$) to + 890 mV (vs. NHE at pH 7; $O_2^{\bullet -}/H_2O_2$), in aqueous media. However, this criterion must be taken into careful consideration due to short half life time (10^{-8} s^{-1}) of superoxide ion in aqueous media and its thermodynamic stability ($K_{dis} = 4.76 \times 10^{20}$, pH = 7.0) [16,17].

For a potential biomimetic complex, a common test to propose a SOD-like mechanism, is the xanthine oxidase bioassay [18,19]. In this procedure, the xanthine/xanthine oxidase system is used as a source of superoxide radicals, which are trapped by the native cytochrome *c*. When the SOD enzyme or a biomimetic compound is added in the assay, the reduction of cytochrome *c* presents a decrease, associated to the disproportion of superoxide, followed spectrophotometrically at 550 nm. The change in absorbance value is related to the SOD activity referenced to enzyme. Nevertheless, this method has several disadvantages, including the use of expensive reagents, highly controlled conditions and interferences such as the chemical interactions between the compound of interest with the radical generator (xanthine/xanthine oxidase) and the radical trapping agent (cytochrome *c*). Furthermore, in this bioassay, the already mentioned short half-life of the superoxide in aqueous solution is not considered, making a non-accurate SOD activity measurement. In the literature, several authors have reported SOD activity for copper complexes, proposing a correlation with the redox potential values of the couple Cu(II)/Cu(I) [20–39]. However, in these studies systematic changes in redox potentials associated to electronic effects of ligands, and the stability of the $O_2^{\bullet -}$ in a reaction media that guarantee the reactivity of this radical is exclusively related to the metal complex. The aforementioned, encouraged us to synthesize tunable redox potential Cu(II) complexes $[Cu(N\text{-}N)_2(X)]^+$, (N-N) = substituted 1,10-phenanthroline and X = Cl^- or NO_3, (1,10-phenantroline = 1,10-phen) see Scheme 1, in order to study the disproportion of $O_2^{\bullet -}$ originated by electrogenerated species $[Cu(N\text{-}N)_2]^+$ in dimethylsufoxide (DMSO) as a function of the electronic changes in the metal center (through redox potential values). This results establish the basis for a new simple tool pointing to SOD-like mechanism, which can be used as a quick guide test, for compounds before being proven in biological assays.

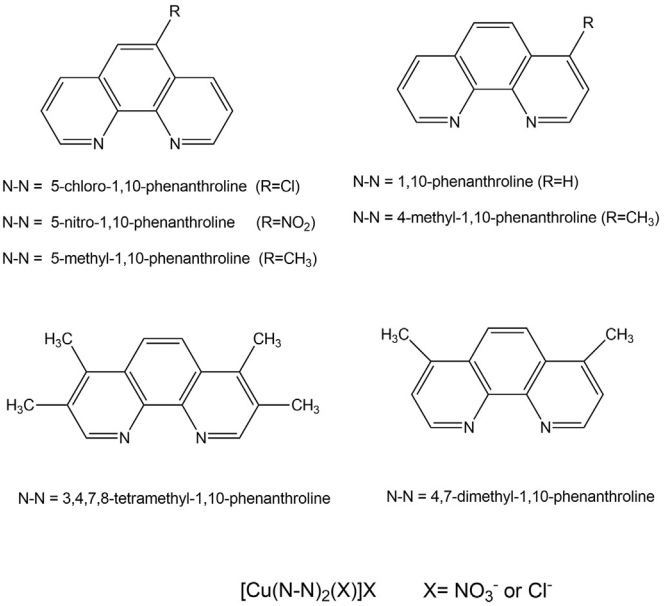

Scheme 1. Bis-chelate substituted 1,10-phenanthroline (N-N) Cu(II) complexes, 1,10-phenanthrolile = 1,10-phen.

2. Methodology

2.1. Chemicals

All chemicals and solvents used were synthetic grade, purchased from the commercial source and used without further purification.

2.2. Synthesis of the complexes $[Cu(II)(N\text{-}N)_2(X)]X$

The synthesis of metal complexes was carried out by dissolving 0.1 mmol of $Cu(NO_3)_2 \cdot 2.5\ H_2O$ or $CuCl_2 \cdot 2H_2O$ in 5 mL of anhydrous ethanol. Then it was added dropwise to the metallic salt solution 0.2 mmol of each (N-N) ligand previously dissolved in 5 mL of anhydrous ethanol. In some cases, the ligand solution was heated at 70 °C for a complete dissolution; a color change from blue to green was observed. The reaction mixture was heated and stirred for 2 h. Solvent was removed by slow evaporation until a powder was observed. The product was filtered and washed with diethyl ether.

2.2.1. $[Cu(1,10\text{-}phen)_2(NO_3)]NO_3 \cdot H_2O$

IR (KBr, cm^{-1}); ν(C=C) + ν(C=N) 1627, 1520, ν(=C-H) 3057, ν(C=C) $_{ring}$ 1605, 1586, 1493, ν_s(N=O) 1315, $\nu_a(NO_2)$ 1330, NO_3^- ionic ν_3(E′) 1383, ν(Cu-N) 202, 278, 351, 431, ν(Cu-O) 403sh. UV–Vis (DMSO) [λ_{max}, nm (ε, M^{-1} cm^{-1})]; 700 (56), 1000 (25). Diffuse reflectance λ_{max}: 792 nm. Λ(DMSO) = 81 S cm^2 mol^{-1}. Anal. Calc. for $CuC_{24}H_{18}N_6O_7$ (MW = 565 g/mol) %C, 50.93; %H, 3.20; %N, 14.84. Found: %C, 50.91; %H, 3.21; %N, 14.80. Mass spectrum FAB(+) *m/z* = 485, $[Cu(1,10\text{-}phen)_2NO_3]^+$, *m/z* = 423 $[Cu(1,10\text{-}phen)_2]^+$.

2.2.2. $[Cu(3,4,7,8\text{-}tetramethyl\text{-}1,10\text{-}phen)_2(NO_3)]NO_3 \cdot H_2O$

IR (KBr, cm^{-1}); ν(C=C) + ν(C=N) 1620,1529, ν(C=C) $_{ring}$ 1596, 1529, 1432, ν(=C-H) 3043, ν(-C-H) 2964, 2923, ν_s(N=O) 1376, $\nu_a(NO_2)$ 1358, NO_3^- ionic ν_3(E′) 1383, ν(Cu-N) 209, 280, 351, 417, ν(Cu-O) 417 sh. UV–Vis(DMSO) [λ_{max}, nm (ε, M^{-1} cm^{-1})]; 709 (55), 920 (34). Diffuse reflectance λ_{max}: 745, 910 (shoulder) nm. Λ(DMSO) = 70 S cm^2 mol^{-1}. Anal. Calc. for $CuC_{32}H_{34}N_6O_7$ (MW = 678 g/mol) %C, 56.67; %H, 5.03; %N, 12.39. Found: %C, 56.50; %H, 5.04; %N, 12.40. Mass spectrum FAB(+) *m/z* = 597 $[Cu(3,4,7,8\text{-}tetramethyl\text{-}1,10\text{-}phen)_2(NO_3)]^+$, *m/z* = 535 $[Cu(3,4,7,8\text{-}tetramethyl\text{-}1,10\text{-}phen)_2]^+$.

2.2.3. $[Cu(5\text{-}methyl\text{-}1,10\text{-}phen)_2(NO_3)]NO_3 \cdot 3\ H_2O$

IR (KBr, cm^{-1}); ν(C=C) ν(C=N) 1624, 1522, ν(C=C) $_{ring}$ 1602, 1585, 1487, ν(=C-H) 3055, ν(-C-H) 2918, ν_s(N=O) 1336, $\nu_a(NO_2)$ 1363, NO_3^- ionic ν_3(E′) 1379, ν(Cu-N) 210, 279, 352, 429, ν(Cu-O) 419 sh. UV–Vis(DMSO) [λ_{max}, nm (ε, M^{-1} cm^{-1})]; 697 (46), 1018 (21). Diffuse reflectance λ_{max}: 758, 981 nm. Λ(DMSO) = 50 S cm^2 mol^{-1}. Anal. Calc. for $CuC_{26}H_{26}N_6O_9$ (MW = 630 g/mol) %C, 49.56; %H, 4.15; %N, 13.32. Found: %C, 49.60; %H, 4.17; %N, 13.25. Mass spectrum FAB(+) *m/z* = 513 $[Cu(5\text{-}methyl\text{-}1,10\text{-}phen)_2(NO_3)]^+$, *m/z* = 451 $[Cu(5\text{-}methyl\text{-}1,10\text{-}phen)_2]^+$.

2.2.4. $[Cu(4\text{-}methyl\text{-}1,10\text{-}phen)_2(NO_3)]NO_3 \cdot 2H_2O$

IR (KBr, cm^{-1}); ν(C=C) ν(C=N) 1624, 1520, ν(C=C) $_{ring}$ 1602, 1587, 1487, ν(=C-H) 3059, 3002, ν(-C-H) 2920, ν_s(N=O) 1358, $\nu_a(NO_2)$ 1336, NO_3^- ionic ν_3(E′) 1379, ν(Cu-N) 212, 279, 350, 417, ν(Cu-O) 426 sh. UV–Vis(DMSO) [λ_{max}, nm (ε, M^{-1} cm^{-1})]; 700 (54), 992 (26). Diffuse reflectance λ_{max}: 738 nm. Λ(DMSO) = 67 S cm^2 mol^{-1}. Anal. Calc. for $CuC_{26}H_{24}N_6O_8$ (MW = 612 g/mol) %C, 51.02; %H, 3.95; %N, 13.73. Found: %C, 51.10; %H, 4.0; %N, 13.70. Mass spectrum FAB(+) *m/z* = 513 $[Cu(4\text{-}methyl\text{-}1,10\text{-}phen)_2(NO_3)]^+$, *m/z* = 451 $[Cu(4\text{-}methyl\text{-}1,10\text{-}phen)_2]^+$.

2.2.5. $[Cu(4,7\text{-}dimethyl\text{-}1,10\text{-}phen)_2(NO_3)]NO_3$

IR (KBr, cm^{-1}); ν(C=C) ν(C=N) 1621, 1523, ν(C=C) $_{ring}$ 1608, 1577, 1458, ν(=C-H) 3084, 3062, ν(-C-H) 2928, 2962, 2921, ν_s(N=O)

1363, $\nu_a(NO_2)$ 1335, NO_3^- ionic $\nu_3(E')$ 1355, ν(Cu-N) 220, 282, 351, 419, ν(Cu-O) 419 sh. UV–Vis(DMSO) [λ_{max}, nm (ε, $M^{-1}\,cm^{-1}$)]; 701 (64) 960 (32). Diffuse reflectance λ_{max}: 749, 1009 nm. Λ(DMSO) = 66 S $cm^2\,mol^{-1}$. Anal. Calc. for $CuC_{28}H_{24}N_6O_6$ (MW = 604 g/mol) %C, 55.67; %H, 4.00; %N, 13.91. Found: %C, 55.57%H, 4.02; %N, 13.98. Mass spectrum FAB(+) *m/z* = 541 [Cu(4,7-dimethyl-1,10-phen)$_2$(NO$_3$)]$^+$, *m/z* = 479 [Cu(4,7-dimethyl-1,10-phen)$_2$]$^+$.

2.2.6. [Cu(5-chloro-1,10-phen)$_2$(NO$_3$)]NO$_3$

IR (KBr, cm^{-1}); ν(C=C) ν(C=N) 1614, 1581, ν(C=C) $_{ring}$ 1604, ν(=C-H) 3043, $_s$(N=O) 1340, $\nu_a(NO_2)$ 1330, NO_3^- ionic $\nu_3(E')$ 1380, ν(Cu-N) 210, 280, 350, 420, ν(Cu-O) 420 sh. UV–Vis(DMSO) [λ_{max}, nm (ε, $M^{-1}\,cm^{-1}$)]; 700 (40) 1060 (15). Diffuse reflectance λ_{max}: 790, 860 nm. Λ(DMSO) = 65 S $cm^2\,mol^{-1}$. Anal. Calc. for $CuC_{24}Cl_2H_{14}N_6O_6$ (MW = 616. g/mol) %C, 46.72; %H, 2.28; %N, 13.62. Found: %C, 46.70; %H, 2.26; %N, 13.60. Mass spectrum FAB(+) *m/z* = 553 [Cu(5-Cl-1,10-phen)$_2$Cl]$^+$, *m/z* = 491[Cu(5-Cl-1,10-phen)$_2$]$^+$.

2.2.7. [Cu(5-nitro-1,10-phen)$_2$(NO$_3$)]NO$_3$

IR (KBr, cm^{-1}); ν(C=C) ν(C=N) 1624, 1512, ν(C=C) $_{ring}$ 1606, 1584, 1423, ν(=C-H) 3080, 3061, ν(ϕ-NO_2)$_{sy}$ 1512, ν(ϕ-N=O) 1535; ν(ϕ-NO_2)$_{as}$ 1368, ν_s(N=O) 1345, $\nu_a(NO_2)$ 1336, NO_3^- ionic $\nu_3(E')$ 1380, ν(Cu-N) 213, 278, 351, 419, ν(Cu-O) 418 sh. UV–Vis(DMSO) [λ_{max}, nm (ε, $M^{-1}\,cm^{-1}$)]; 702 (49) 1083(19). Diffuse reflectance λ_{max}: 790, 864 nm. Λ(DMSO) = 70 S $cm^2\,mol^{-1}$. Anal. Calc. for $CuC_{24}H_{14}N_8O_{10}$ (MW = 637 g/mol) %C, 45.18; %H, 2.21; %N, 17.56. Found: %C, 45.22; %H, 2.23; %N, 17.60. Mass spectrum FAB(+) *m/z* = 575 [Cu(5-nitro-1,10-phen)$_2$(NO$_3$)]$^+$, *m/z* = 513 [Cu(5-nitro-1,10-phen)$_2$]$^+$.

2.2.8. [Cu(1,10-phen)$_2$Cl]Cl 2H$_2$O

IR (KBr, cm^{-1}); ν(C=C) + ν(C=N) 1625, 1517, ν(C=C) $_{ring}$ 1604, 1584, 1427, ν(=C-H) 3052. ν(Cu-N) 204, 279, 352, 429, ν(Cu-Cl) 281 sh. UV–Vis(DMSO) [λ_{max}, nm (ε, $M^{-1}\,cm^{-1}$)]; 739 (100), 949 (72). Diffuse reflectance λ_{max}: 824 nm. Λ(DMSO) = 25 S $cm^2\,mol^{-1}$. Anal. Calc. for $CuC_{24}H_{20}N_4Cl_2O_2$ (MW = 530 g/mol) %C, 54.29; %H, 3.79; %N, 10.55. Found: %C, 54.10; %H, 3.81; %N, 10.50. Mass spectrum FAB(+) *m/z* = 458 [Cu(1,10-phen)$_2$Cl]$^+$, *m/z* = 423 [Cu(1,10-phen)$_2$]$^+$.

2.2.9. [Cu(3,4,7,8-tetramethyl-1,10-phen)$_2$Cl]Cl 5H$_2$O

IR (KBr, cm^{-1}); ν(C=C) + ν(C=N) 1620,1527, ν(C=C) $_{ring}$ 1597, 1430, ν(Cu-N) 211, 281, 352, 419, ν(Cu-Cl) 254 sh. UV–Vis(DMSO) [λ_{max}, nm (ε, $M^{-1}\,cm^{-1}$)]; 742 (140), 941 (110). Diffuse reflectance λ_{max}: 745 nm. Λ(DMSO) = 26 S $cm^2\,mol^{-1}$. Anal. Calc. for $CuC_{32}H_{42}N_4Cl_2O_5$· (MW = 697 g/mol) %C, 55.13; %H, 6.07; %N, 8.03. Found: %C, 55.10; %H, 6.01; %N, 8.15. Mass spectrum FAB(+) *m/z* = 570 [Cu(3,4,7,8-tetramethyl-1,10-phen)$_2$Cl]$^+$, *m/z* = 535 [Cu(3,4,7,8-tetramethyl-1,10-phen)$_2$]$^+$.

2.2.10. [Cu(5-methyl-1,10-phen)$_2$Cl]Cl 5H$_2$O

IR (KBr, cm^{-1}); ν(C=C) ν(C=N) 1624, 1520, ν(C=C) $_{ring}$ 1602, 1585, 1485,1425, ν(=C-H) 3056, ν(Cu-N) 211, 279, 353, 430, ν(Cu-Cl) 299 sh. UV–Vis(DMSO) [λ_{max}, nm (ε, $M^{-1}\,cm^{-1}$)]; 736 (105), 949 (77). Diffuse reflectance λ_{max}, nm; 775, 943. Λ(DMSO) = 50 S $cm^2\,mol^{-1}$. Anal. Calc. for $CuC_{26}H_{30}N_4Cl_2O_5$ (MW = 612 g/mol) %C, 50.94; %H, 4.93; %N, 9.13. Found: %C, 50.80; %H, 4.96; %N, 9.10. Mass spectrum FAB(+) *m/z* = 486 [Cu(5-methyl-1,10-phen)$_2$Cl]$^+$, *m/z* = 451 [Cu(5-methyl-1,10-phen)$_2$]$^+$.

2.2.11. [Cu(4-methyl-1,10-phen)$_2$Cl]Cl 4H$_2$O

IR (KBr, cm^{-1}); ν(C=C) ν(C=N) 1623, 1521, ν(C=C) $_{ring}$ 1604, 1588, 1427, ν(=C-H) 3054, (Cu-N) 202, 279, 353, 417, ν(Cu-Cl) 268 sh. UV–Vis(DMSO) [λ_{max}, nm (ε, $M^{-1}\,cm^{-1}$)]; 736 (153), 949 (114). Diffuse reflectance λ_{max}: 745, 1014 nm. Λ(DMSO) = 25 S $cm^2\,mol^{-1}$. Anal. Calc. for $CuC_{26}H_{28}N_4Cl_2O_4$ (MW = 594 g/mol) %C,52.28; %H, 4.74; %N, 9.41. Found: %C, 52.32; %H, 4.78; %N, 9.40. Mass spectrum FAB(+) *m/z* = 486 [Cu(4-methyl-1,10-phen)$_2$Cl]$^+$, *m/z* = 451 [Cu(4,7-dimethyl-1,10-phen)$_2$]$^+$.

2.2.12. [Cu(4,7-dimethyl-1,10-phen)$_2$Cl]Cl 2H$_2$O

IR (KBr, cm^{-1}); ν(C=C) ν(C=N) 1621, 1522, ν(C=C) $_{ring}$ 1605, 1577, 1423, ν(=C-H) 3040, ν(Cu-N) 213, 282, 351, 419, ν(Cu-Cl) 265 sh. UV–Vis(DMSO) [λ_{max}, nm (ε, $M^{-1}\,cm^{-1}$)]; 745 (206) 950 (155). Diffuse reflectance λ_{max}: 735, 1012 nm. Λ(DMSO) = 27 S $cm^2\,mol^{-1}$. Anal. Calc. for $CuC_{28}H_{28}N_4Cl_2O_2$ (MW = 586 g/mol) %C, 57.29; %H, 4.80; %N, 9.54. Found: %C, 57.02; %H, 4.77; %N, 9.59. Mass spectrum FAB(+) *m/z* = 514 [Cu(4,7-dimethyl-1,10-phen)$_2$Cl]$^+$, *m/z* = 479 [Cu(4-methyl-1,10-phen)$_2$]$^+$.

2.2.13. [Cu(5-nitro-1,10-phen)$_2$Cl]Cl H$_2$O

IR (KBr, cm^{-1}); ν(C=C) ν(C=N) 1625, 1518, ν(C=C) $_{ring}$ 1606, 1585, 1420, ν(=C-H) 3057, ν(ϕ-NO_2)$_{sy}$ 1518, ν(ϕ-N=O) 1532, ν(Cu-N) 208, 280, 350, 419, ν(Cu-O) 468 sh. UV–Vis(DMSO) [λ_{max}, nm (ε, $M^{-1}\,cm^{-1}$)]; 738 (74) 957 (56). Diffuse reflectance λ_{max}: 794, 860 nm. Λ(DMSO) = 32 S $cm^2\,mol^{-1}$. Anal. Calc. for $CuC_{24}H_{16}N_6Cl_2O_5$ (MW = 602 g/mol) %C, 47.81; %H, 2.67; %N, 13.94. Found: %C, 47.90; %H, 2.68; %N, 13.90. Mass spectrum FAB(+) *m/z* = 548 [Cu(5-nitro-1,10-phen)$_2$Cl]$^+$, *m/z* = 513 [Cu(5-nitro-1,10-phen)$_2$]$^+$.

2.3. Physical measurements

Elemental analyses were performed in a Fisons Instruments Analyzer model EA 1108, using a sulfanilamide standard. Mid-IR spectra were recorded on KBr disks, using a Nexus Thermo Nicolet Spectrophotometer. Far-IR was measured using a Bruker Vertex 70 Spectrophotometer. Solution and solid-state UV–Vis-NIR spectra (40000–4000 cm^{-1}) were obtained on a Cary-5E Varian Spectrophotometer. Conductivity measurements were performed using a YSI 3200 Conductimeter with parallel plates with cell constant of 1 cm^{-1}. Mass spectra were obtained in a JEOL MSTATION, JMS-700, mass spectrometer using fast atomic bombarded FAB(+) ionization method. Temperature of ionization source was 25 °C, with voltage of 6 KeV and current of 5 mA. The matrix employed was nitrobenzyl alcohol.

2.4. Single crystal X-ray diffraction analysis

A single crystal of complex [Cu(3,4,7,8-tetramethyl-1,10-phen)$_2$(NO$_3$)](NO$_3$)·H$_2$O was mounted on glass fiber to be studied with an Oxford Diffraction Gemini "A" diffractometer, equipped with a CCD area detector, a sealed tube X-ray source ($\lambda_{MoK\alpha}$ = 0.71073 Å) and monochromator of graphite. A data sets consisted of frames of intensity collected with a frame width of 1° in ω, a counting time of 12.5 s/frame, and a crystal-to-detector distance of 55.00 mm. The double pass method of scanning was used to exclude any noise. The collected frames were integrated by using an orientation matrix determined from the narrow frame scans. CrysAlis Pro and CrysAlis RED software packages [40] were used for data collection and data integration. Analysis of the integrated data did not reveal any decay. Final cell parameters were determined by a global refinement of reflections. Collected data were corrected for absorbance by using analytical numeric absorption correction [41], using a multifaceted crystal model based on expressions upon the Laue symmetry using equivalent reflections. Structure solution and refinement were carried with the programs SHELXS-2014 and SHELXL-2014 respectively [42].; for molecular graphics: ORTEP-3 for Windows [43]; and the software used to prepare material for publication: WinGX [44]. Full-matrix least-squares refinement was carried out by minimizing $(Fo^2 - Fc^2)^2$. All non-hydrogen atoms were refined anisotropically. For H atom of the water group (H-O) were located in a difference map and refined isotropically with Uiso(H) = 1.5 for H-O. H atoms attached to C atoms were placed in geometrically idealized

Table 1
Crystal data and structure refinement for $[Cu(3,4,7,8,tm\text{-}1,10\text{-}phen)_2NO_3]NO_3 \cdot H_2O$.

Empirical formula	$C_{32}\ H_{34}\ Cu\ N_6\ O_7$
Formula weight	678.19
Temperature	130(2) K
Wavelength	0.71073 Å
Crystal system	Monoclinic
Space group	P 21/c
Unit cell dimensions	a = 7.723(6) Å b = 23.20(2) Å c = 16.859(11) Å β = 95.772(6)°
Volume	3005.8(4) $Å^3$
Z	4
Density (calculated)	1.499 Mg/m^3
Absorption coefficient	0.787 mm^{-1}
F(000)	1412
Crystal size	0.400 × 0.120 × 0.070 mm^3
Theta range for data collection	3.411 to 29.471°
Index ranges	−10 ≤ h ≤ 10, −26 ≤ k ≤ 30, −21 ≤ l ≤ 12
Reflections collected	15,093
Independent reflections	7159 [R(int) = 0.0423]
Completeness to theta = 25.242°	99.8%
Refinement method	Full-matrix least-squares on F^2
Data/restraints/parameters	7159/0/429
Goodness-of-fit on F^2	1.049
Final R indices [I > 2sigma (I)]	R1 = 0.0496, wR2 = 0.0925
R indices (all data)	R1 = 0.0802, wR2 = 0.1080
Largest diff. peak and hole	0.443 and −0.500 e.$Å^{-3}$

positions and refined as riding on their parent atoms, with C—H = 0.95 and 0.98 Å with U_{iso} (H) of 1.2U_{eq}(C) and 1.5U_{eq}(C) for aromatic and methyl groups respectively. Crystal data and experimental details of the structure determinations are listed in Table 1.

2.5. Electrochemical studies

Electrochemical experiments were carried out using a Potentiostat/Galvanostat BioLogic SP-50. A typical three-electrode array was employed for all electrochemical measurements. All Complexes were dried at 110 °C in a vacuum oven 24 h before its electrochemical characterization. The concentration of each complex was 1×10^{-3} M in DMSO (99.7% Extra Dry over molecular sieve Acros Organics) solution in the presence of Tetrabutylammonium hexafluorophosphate $TBAPF_6$ 0.1 M. To avoid water into the electrochemical experiments, the DMSO solution containing the complex was also heated 2 h at 90 °C. After that, the flask was stoppered and cooled at room temperature. A platinum disk (ϕ = 1.6 mm) was used as working electrode. A homemade Ag/Ag^+ (AgNO3 0.1 M in DMSO) reference electrode was employed. Prior to be used, the working electrode was polished with diamond powder, rinsed with distilled water and sonicated for 2 min. Before each measurement the electrode was polished with α-alumina (0.6 μm), rinsed with distilled water and dried. The solutions were bubbled with nitrogen before each experiment. All potential values are reported vs the couple Fc/Fc^+, according to the IUPAC convention [45]. Cyclic voltammetry was performed from open circuit potential to negative direction with variable scan rate from 10 to 1000 mV s^{-1}. Ohmic drop compensation was applied using the current interrupt method. Single pulse chronoamperometry experiments were obtained stepping the potential from open circuit potential ($E_{i=0}$) to a potential (E_1) where the electrochemical process is limited by diffusion, established from CV experiments. A time width (τ) of 5 s was used.

2.6. Reaction between Cu(II) complexes with electro-generated superoxide from molecular oxygen

Air from a KNF laboport mini pump was passed through a sealed trap containing a molecular sieve. Then the dry air was bubbled to a DMSO solution + $TBAPF_6$ 0.1 M by 10 min. Electrochemical experiments of saturated O_2 solution in the presence and in the absence of metal complex 1 mM were carried out. Additionally, experiments for oxygen reduction with additions of water were obtained to explore the effect of a proton donor in the disproportionation of superoxide anion.

2.7. Theoretical calculations

The geometry optimization of metal complexes was performed using the hybrid meta-GGA functional m06-2x [46–50] with a 6-31g (d, p) basis set in the gas phase and with a PMC solvent model (DMSO). This functional has proved adequate in representing both the structure, energetics and stability of first-row transition metal complexes as we have previously shown [51–53]. Charge and multiplicity values for complexes were + 1/1. Vibrational frequencies were obtained and no negative values found, confirming the convergence of the optimization. All quantum mechanics calculations were performed using the D.01 revision of Gaussian 09 [54].

3. Results and discussion

3.1. Solid state characterization of metal complexes $[Cu(II)(N\text{-}N)_2(X)]X$

The reaction between copper salts $Cu(NO_3)_2 \cdot 2.5\ H_2O$ or $CuCl_2\ 2H_2O$ and the 1,10-phenanthroline ligands (N-N) in molar ratio (1:2) yield green powders. IR spectrum of $[Cu(II)(N\text{-}N)_2(X)]X$, (X = NO_3^- or Cl^-) show vibrational frequencies related to the presence of the diiminic ligand N-N and to the nitrate moiety. As example in the compound $[Cu(3,4,7,8\text{-tetramethyl-}1,10\text{-phen})_2(NO_3)]NO_3 \cdot H_2O$, the vibrational frequencies ν(C=C) + ν(C=N) are detected at 1620 and 1529 cm^{-1}. A broad absorption band around 1383 cm^{-1}, attributable to ionic nitrate ν_3(E′) was recorded. The vibrational frequencies ν_s(N=O) and $\nu_a(NO_2)$ at 1376 cm^{-1} and 1358 cm^{-1}, suggest a monodentate coordination mode with the metal center [55–56]. A comparison between IR spectra of the free ligand and metal complex, show a shift to high wavenumber (Δυ) around 10–20 cm^{-1}, in the molecular vibrations $\nu(C=C)_{ring}$ and ν(C=C) + ν(C=N), due to the coordination of the metal center, see Fig. 1. Furthermore, characteristic frequencies in far IR region ν(Cu-O), ν (Cu-N) and ν (Cu-Cl) are detected see SI. IR spectra for all compounds presents similar behavior, see SI.

The coordination of both ions in complexes is also demonstrated by mass spectrometry, where the stable molecular ions (*m/z*) for [Cu(N-

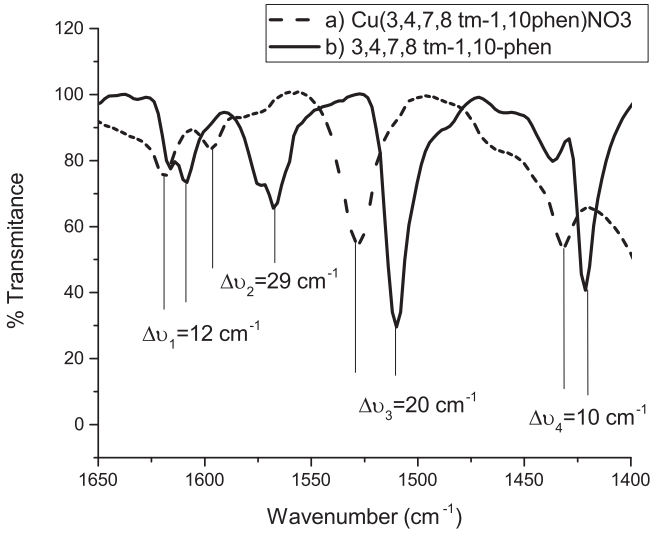

Fig. 1. IR of $[Cu(3,4,7,8\text{-tetramethyl-}1,10\text{-phen})_2(NO_3)]NO_3 \cdot H_2O$ and 3,4,7,8-tetramethyl-1,10-phen.

Table 2
Difusse reflectance spectroscopy data for the complexes $[Cu(N\text{-}N)_2(NO_3)]\ NO_3$ and $[Cu(N\text{-}N)_2Cl]Cl$.

Compound	(d → d) electronic transitions (nm)	Geometry
$[Cu(1,10\text{-phen})_2(NO_3)]NO_3 \cdot H_2O$	792	Distorted trigonal bipyramidal
$[Cu(1,10\text{-phen})_2Cl]Cl\ 2H_2O$	824	Distorted trigonal bipyramidal
$[Cu(3,4,7,8\text{-tetramethyl-1,10-phen})_2(NO_3)]\ NO_3 \cdot H_2O$	745, 910	Distorted square pyramidal
$[Cu(3,4,7,8\text{-tetramethyl-1,10-phen})_2Cl]Cl \cdot 5H_2O$	745	Distorted trigonal bipyramidal
$[Cu(5\text{-methyl-1,10-phen})_2(NO_3)]NO_3 \cdot 3H_2O$	758, 981	Distorted square pyramidal
$[Cu(5\text{-methyl-1,10-phen})_2Cl]Cl\ 5H_2O$	775, 943	Distorted square pyramidal
$[Cu(4\text{-methyl-1,10-phen})_2(NO_3)]NO_3 \cdot 2H_2O$	738	Distorted trigonal bipyramidal
$[Cu(4\text{-methyl-1,10-phen})_2\ Cl]Cl\ 4H_2O$	745, 1014	Distorted square pyramidal
$[Cu(4,7\text{-dimethyl-1,10-phen})_2(NO_3)]NO_3$	749, 1009	Distorted square pyramidal
$[Cu(4,7\text{-dimethyl-1,10-phen})_2Cl]Cl\ 2H_2O$	735, 1012	Distorted square pyramidal
$[Cu(5\text{-chloro-1,10-phen})_2(NO_3)]NO_3$	790, 860	Distorted square pyramidal
$[Cu(5\text{-chloro-1,10-phen})_2Cl]Cl$	792, 863	Distorted square pyramidal

$N)_2(NO_3)]^+$ and $[Cu(N\text{-}N)_2Cl]^+$ are detected, see SI. On the other hand, difusse reflectance in visible region for complexes was also carried out. Based on literature distorted trigonal bipyramidal or distorted square pyramidal geometries arround Cu(II) are proposed, see Table 2 and SI [57,58]. Furthermore, the crystal structure of cationic complex [Cu(1,10-phenatroline)$_2$Cl]$^+$, already reported, allow us to state the geometry with one chloro coordinated to the metal center [59].

3.2. X-ray analysis

The Cu(II) ion in $[Cu(3,4,7,8\text{-tetramethyl-1,10-phen})_2(NO_3)](NO_3) \cdot H_2O$ presents a *cis*-distorted octahedral geometry with a high trigonal bipyramidal distortion. The coordination sphere of the metal ion is constituted by four nitrogen atoms coming from phenanthroline units with Cu-N bond lengths around 1.98 and 2.2 Å. The shortest Cu-O is 2.0316(19) Å and the longest is 2.617(2) Å are within the range of Cu-O bond length found for oxyanion coordinated in a bidentate mode (1.97–2.86 Å). Selected bond distances and angles were compiled in Table 3. Fig. 2 shows the molecular structure of compound $[Cu(3,4,7,8\text{-tetramethyl-1,10-phen})_2(NO_3)]NO_3\ H_2O$, the asymmetric unit includes the coordination compound, a nitrate counter ion and a water molecule as solvate. A dihedral angle of 80.44 (5)° between the phenanthroline units is observed. The intermolecular interactions that keep stable the crystal include hydrogen bonds, π-π and C-H···π interaction. The observed hydrogen bonds O1w-H1d…O3 2.08(4) Å and O1w-H2e…O4 2.07(4) Å are established by coordinated and non-coordinated nitrate ion with the water molecule solvate, forming the $D_2^2(5)$ *motif*. On the other side, the aromatic rings of the 1,10-phenanthrolines participate in π-π interactions with centroid-centroid distances of 3.564 Å and C-H···π interactions with distances of 2.937 Å.

Table 3
Experimental and calculated bond lengths [Å] and angles [°] (using DFT methods) for the compound $[Cu(3,4,7,8\text{-tetramethyl-1,10-phen})_2(NO_3)]NO_3\ H_2O$.

Cu(1)-N(1)	2.003 (2)	2.0435
Cu(1)-N(2)	2.199 (2)	2.0770
Cu(1)-N(3)	2.019 (2)	2.0624
Cu(1)-N(4)	1.986 (2)	2.2425
Cu(1)-O(1)	2.0316 (19)	
N(1)-Cu(1)-N(2)	79.2.7 (8)	80.35
N(1)-Cu(1)-N(3)	96.97 (9)	100.00
N(1)-Cu(1)-N(4)	179.24 (9)	175.54
N(2)-Cu(1)-N(3)	101.30 (8)	99.38
N(2)-Cu(1)-N(4)	100.53 (8)	96.17
N(3)-Cu(1)-N(4)	82.34 (9)	77.71
N(3)-Cu(1)-O(1)	162.69 (8)	
N(4)-Cu(1)-O(1)	92.21 (8)	
N(2)-Cu(1)-O(1)	95.83 (8)	
N(1)-Cu(1)-O(1)	88.55 (8)	

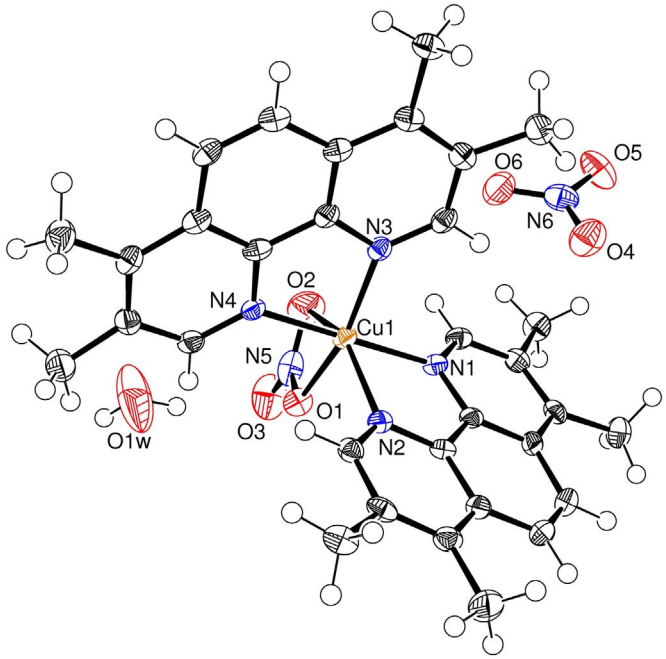

Fig. 2. ORTEP view of $[Cu(3,4,7,8\text{-tetramethyl-1,10-phen})_2(NO_3)]NO_3\ H_2O$. Ellipsoids are shown at the 65% probability level.

3.3. Solution behavior of metal complexes

The electronic spectra of $[Cu(3,4,7,8\text{-tetramethyl-1,10-phen})_2(NO_3)](NO_3) \cdot H_2O$ complex in DMSO solution show two electronic transitions at 709 nm ($\varepsilon = 55\ M^{-1}\ cm^{-1}$) and 920 nm ($\varepsilon = 34\ M^{-1}\ cm^{-1}$) typical of distorted square pyramidal Cu(II) complexes [58]. The presence of two absorption bands for all the complexes in DMSO solution suggest the same geometry. Besides, the range of molar conductance (50 to 81 S $cm^2\ mol^{-1}$) for nitrato complexes is similar than the recorded value for the precursor salt $Cu(NO_3)_2\ 2.5\ H_2O$ in the same conditions ($\Lambda = 45\ \Omega^{-1}\ cm^2\ mol^{-1}$). In the case of chloro complexes, molar conductance values (25–50 S $cm^2\ mol^{-1}$) are in the same range than the $CuCl_2\ 2H_2O$ ($\Lambda = 15.77\ \Omega^{-1}\ cm^2\ mol^{-1}$). The difference in molar conductance values between the two groups of complexes is attributed to the solvation of the anions for 1:1 electrolytes. The above mentioned results allow us to proposed the chemical species $[Cu(N\text{-}N)_2(NO_3)]^+$ in DMSO solution. In the case of choro complexes the ionic structure is considered in this work, however the presence of chemical neutral species such as $[Cu(N\text{-}N)_2(Cl)]Cl$, due to ion pair formation, cannot be discarded.

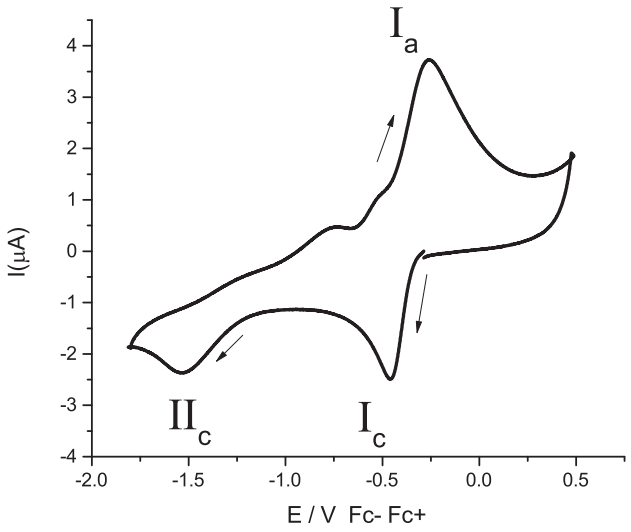

Fig. 3. Cyclic voltammogram of the complex $[Cu(1,10\text{-phen})_2NO_3]^+$ 1×10^{-3} M, in DMSO + $TBAPF_6$ 0.1 M, cathodic direction. Working electrode: Pt. Scan rate = 0.1 V/s.

3.4. Electrochemical behavior of [Cu(N-N)2(X)]X

A typical cyclic voltammogram of $[Cu(1,10\text{-phen})_2NO_3]^+$ in DMSO solution in cathodic direction is shown in Fig. 3. The main processes observed are two reduction signals (Ic and IIc) and one oxidation signal (Ia), with peak potential values E_{pc}(Ic) = − 0.463 V vs Fc-Fc^+, E_{pc}(IIc) = − 1.503 V vs Fc-Fc^+, and E_{pa}(Ia) = − 0.256 V vs Fc-Fc^+. Switching potential experiments ($E_{-\lambda}$), see Fig. 4, were carried out to establish a relationship between signals. A dependence between the oxidation process Ia and the reduction processes Ic and IIc is observed. A more detailed inspection of the series of voltammograms, reveal changes in the shape of signal Ia and in their corresponding potential peak values E_{pa} when the switching potential was increased negatively.

At this point it is reasonable to assume for signals Ic and IIc the reduction processes Cu(II) + 1e → Cu(I) and Cu(I) + 1e → Cu^0. However, for a two consecutive one-electron transfer, the peak current (i_p) and the difference between the potential peak and the half-peak potential [E_p-$E_{p/2}$] should presented similar values (0.067 V for Ic and 0.172 V and for IIc). Considering that both facts are not observed in the voltammograms of complex $[Cu(1,10\text{-phen})_2(NO_3)]^+$, and the absence of a typical anodic metal dissolution signal, the electrochemical reduction Cu(I) + 1e → Cu^0 must be neglected. Hence, according to the literature, it is possible to propose the following mechanism, where the equilibria between adsorbed and soluble species is presented [60–61].

$$[Cu^{II}(1,10\text{-phen})_2(NO_3)]^+ + 1e^- \rightleftharpoons [Cu^{I}(1,10\text{-phen})_2]^+ + NO_3^-$$

$$\downarrow\uparrow \qquad\qquad \downarrow\uparrow$$

$$[Cu^{II}(1,10\text{-phen})_2(NO_3)]^+_{(ads)} + 1e^- \rightarrow [Cu^{I}(1,10\text{-phen})_2]^+_{(ads)} + NO_3^-$$

An electron transfer $[Cu^{II}(1,10\text{-fen})_2NO_3]^+ + 1e^- \rightarrow [Cu^{I}(1,10\text{-fen})_2]^+ + NO_3^-$, controlled by diffusion is considered for processes I. A second reduction, of chemical species adsorbed at electrode $[Cu^{II}(1,10\text{-fen})_2(NO_3)]^+_{(ads)} + 1e^- \rightarrow [Cu^{I}(1,10\text{-phen})_2]^+_{(ads)}$ occurs at potential peak value E_{pc}(IIc). Due to the current increase for signal Ia is observed when the switched potential reaches values close to E_{pc}(IIc), see Fig. 4, the backward oxidation process for $[Cu^{I}(1,10\text{-phen})_2]^+_{(ads)}$, must be taking place close to the E_{pa}(Ia) value. To prove this mechanism, the electrochemical response of the complex employing a glassy carbon electrode was carried out, where signal IIc is not recorded and signal Ia show a diminution. Moreover, signal Ic did not show changes for both electrodes, see SI. The electrochemical response, of other copper complex containing a substituted 1,10-phenathroline can be used as evidence for the mechanism. Fig. 5 shows a variable switching potential study ($E_{-\lambda}$) for the $[Cu(3,4,7,8\text{-tetramethyl-}1,10\text{-fen})_2NO_3]^+$ complex. It can be observed only the reduction process Ic with its corresponding oxidation signal Ia. In the anodic signal, a change in its shape and in its potential peak value (Epa) is detected when $E_{-\lambda}$ value was increased negatively, due low adsorption of Cu(II) species. Hence a comparison between the electrochemical responses of $[Cu(1,10\text{-phen})_2NO_3]^+$ and $[Cu(3,4,7,8\text{-tetramethyl-}1,10\text{-phen})_2NO_3]^+$ complexes also confirm the proposed mechanism, indicating that bulky cationic complexes $[Cu(N\text{-}N)_2(X)]^+$ diminishes the amount of species adsorbed at the electrode surface.

To explore kinetics and thermodynamic aspects for process I, cyclic voltammetry experiments at different scan rates for the complex $[Cu(1,10\text{-phen})_2NO_3]^+$, with a low switching potential window were performed. The results of this series of voltammograms are presented in Fig. 6, which is typical response of a quasi-reversible system.

Furthermore, it was added ferrocene 1×10^{-3} M, as internal standard. Fig. 7 shows the cyclic voltammograms of the $[Cu(1,10\text{-phen})_2(NO_3)]^+$ + ferrocene mixture. It can be observed that as the scanning rate is increased, the value of ΔEp increase in process I, while for the Fc/Fc^+, this parameter does not present significant variations. It can be also inferred from the peak currents, the difference between the diffusion coefficients for ferrocene and the cationic [Cu(1,10-

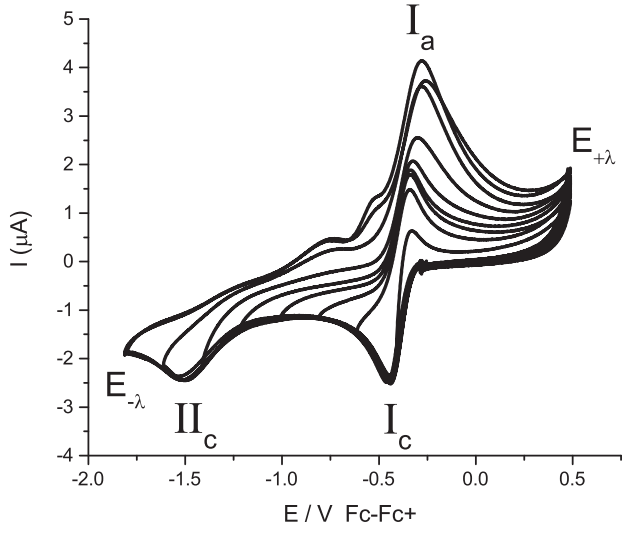

Fig. 4. Switching inversion potential experiments of $[Cu(1,10\text{-fen})_2(NO_3)]^+$ 1×10^{-3} M, in DMSO + $TBAPF_6$ 0.1 M, cathodic direction. Working electrode: Pt, scan rate = 0.1 V/s.

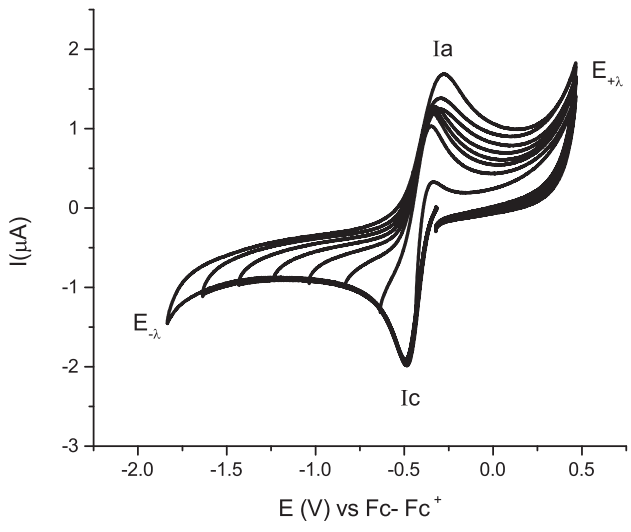

Fig. 5. Variable switching potential experiments ($E_{-\lambda}$) of $[Cu(3,4,7,8\text{-tetramethyl-}1,10\text{-phen})_2(NO_3)]^+$, 1×10^{-3} M, in DMSO + $TBAPF_6$ 0.1 M, cathodic direction. Working electrode: Pt, scan rate = 0.1 V/s.

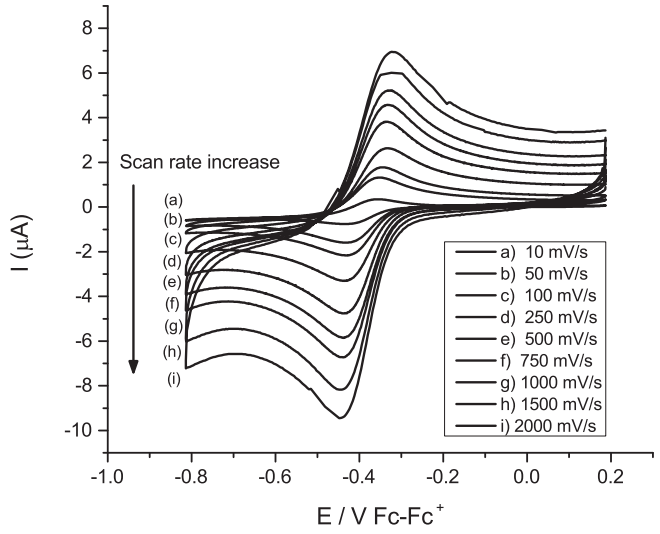

Fig. 6. Cyclic voltammogram of $[Cu(1,10\text{-phen})_2NO_3]^+$ complex 1×10^{-3} M in DMSO + $TBAPF_6$ 0.1 M, cathodic direction. Working electrode: Pt. Scan rate from 0.01 to 1 V/s.

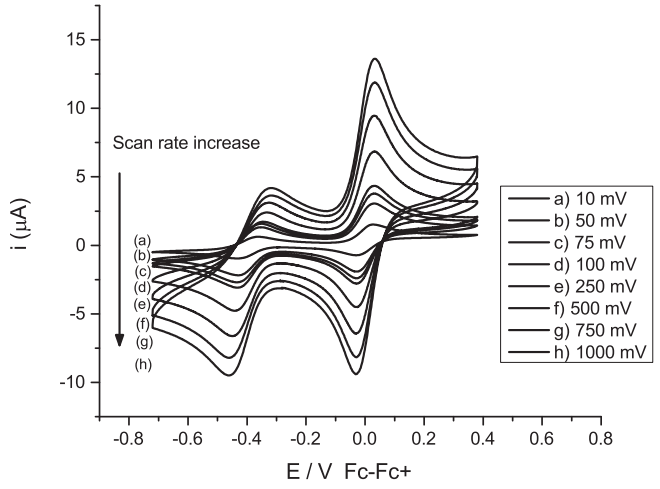

Fig. 7. Cyclic voltammograms of $[Cu(1,10\text{-phen})_2NO_3]^+$ complex 1×10^{-3} M in DMSO + $TBAPF_6$ 0.1 M, cathodic direction in the presence of ferrocene 1×10^{-3} M. Working electrode: Pt. Scan rate from 0.01 to 1 V/s.

fen)$_2NO_3]^+$ complex.

The diffusion coefficient was calculated using one step chronoamperometry experiments, selecting potentials based on the voltammograms, corresponding to the reduction $[Cu^{II}(1,10\text{-fen})_2\ NO_3]^+ + 1e^- \rightarrow [Cu^{I}(1,10\text{-fen})_2]^+ + NO_3^-$. The potential was stepped from open circuit potential (E_i) to potential value where the reduction process is limited by diffusion $E_1 = -0.50$ V vs Fc-Fc$^+$. According to Cottrell's law, a linear relationship I(t) vs $t^{-1/2}$ was obtained, with the equation $I(t) = -3.773 \times 10^{-7}\, t^{-1/2} + 3.66 \times 10^{-8}$ and a correlation coefficient r = 0.998. From the slope $m = (nFAD_0^{1/2}C_0^*)/\pi^{1/2}$, a diffusion coefficient value of 2.76×10^{-6} cm^2/s was obtained. Subsequently, the apparent heterogeneous electron transfer rate constant (k_{app}) was calculated using Nicholson's method [62] involving the dimensionless parameter Ψ and ΔEp values, obtained from cyclic voltammetry experiments and different scan rates. The relationship between Ψ and k_{app} is presented in Eq. (4):

$$\Psi = k_{app}[\pi D_0 n\nu F/RT]^{-1/2} \quad (4)$$

where n is the number of transferred electrons; ν is the scan rate, V/s, F is the Faraday constant; R is the ideal gas constant and T the temperature. Kinetic parameter values, Ψ, for each ΔEp value were taken from the literature [62]. In this case the graph Ψ vs $[\pi D_0 nF\upsilon/(RT)]^{-1/2}$, gives the equation y = 0.0025x + 0.035 r = 0.99, with a k_{app} value of 2.5×10^{-3} cm s^{-1}. The electrochemical behavior of the other compounds synthetized in this work, was studied in the same manner. A summary of the main parameters obtained for the reduction $[Cu^{II}(N\text{-}N)_2(X)]^+ + 1e \rightarrow [Cu^{I}(N\text{-}N)_2]^+ + X^-$ is presented in Table 4. Half wave potential ($E_{1/2}$) differences are observed, due to the π-acceptor character of the ligands, as a function of their pKa values. According to the literature the complexes presented a quasi-reversible behavior. See Table 4 [62,63].

Fig. 8 shows the half wave potential plot ($E_{1/2}$), measured in DMSO, for the reduction process $[Cu^{II}(N\text{-}N)_2NO_3]^+ + 1e^- \rightarrow [Cu^{I}(N\text{-}N)_2]^+ + NO_3^-$ vs the free ligand pKa. A linear relationship was found with an equation $E_{1/2} = -32pKa - 233mV$ with a correlation coefficient r = 0.98, where compounds containing ligands with low pKa values present less negative half-wave potentials. This correlation indicates that the pKa of the ligand contribute in the control of the half wave potential of the complexes, being a π-acceptor character associated with the effect of substituents of diiminic ligands [64]. In the case of chloro complexes the electrochemical reduction from Cu(II) to Cu(I) a linear relationship $E_{1/2} = -22pKa - 324mV$ with a correlation a poor coefficient r = 0.75 was obtained, not considering the complex with the ligand 4,7-dimethyl-1,10-phen. The changes in $E_{1/2}$ values

Table 4
Do, $E_{1/2}$ for redox couple $[Cu(N\text{-}N)_2X]^+/[Cu(N\text{-}N)_2]^+$, k_{app} values, current ratio i_{O2CuL2}/i_{O2} for O_2 reduction (superoxide electrochemical DISP) and pKa values of non-coordinated ligands.

Cationic complex	Do (cm^2/s)	$E_{1/2}$[a] (mV)	k_{app} ($cm\ s^{-1}$)	pKa[b]	i_{O2CuL2}/i_{O2}
$[Cu(4,7\text{-dimethyl-}1,10\text{-phen})_2NO_3]^+$	4.15×10^{-6}	−432	0.0055	5.95	1.37
$[Cu(3,4,7,8\text{-tetramethyl-}1,10\text{-phen})_2NO_3]^+$	1.44×10^{-6}	−426	0.0016	5.81	1.28
$[Cu(5\text{-methyl-}1,10\text{-phen})_2NO_3]^+$	2.48×10^{-6}	−414	0.0027	5.27	1.48
$[Cu(4\text{-methyl-}1,10\text{-phen})_2NO_3]^+$	2.12×10^{-6}	−415	0.0035	5.49	1.46
$[Cu(1,10\text{-phen})_2NO_3]^+$	2.76×10^{-6}	−384	0.0025	4.93	1.37
$[Cu(5\text{-nitro-}1,10\text{-phen})_2NO_3]^+$	1.68×10^{-6}	−338	0.0036	3.22	1.11
$[Cu(5\text{-Chloro-}1,10\text{-phen})_2NO_3]^+$	1.32×10^{-6}	−358	0.0029	4.07	1.08
[c]$[Cu(3,4,7,8\text{-tetramethyl} - 1.10\text{-phen})_2Cl]^+$	2.41×10^{-6}	−448	0.0025	5.81	
[c]$[Cu(4,7\text{-dimethyl-}1,10\text{-phen})_2Cl]^+$	2.68×10^{-6}	−503	0.0036	5.95	
[c]$[Cu(5\text{-methyl-}1,10\text{-phen})_2Cl]^+$	1.58×10^{-6}	−446	0.0033	5.27	
[c]$[Cu(4\text{-methyl-}1,10\text{-phen})_2Cl]^+$	2.16×10^{-6}	−451	0.0035	5.49	
[c]$[Cu(1,10\text{-phen})_2Cl]^+$	2.56×10^{-6}	−450	0.0053	4.93	
[c]$[Cu(5\text{-chloro-}1,10\text{-phen})_2Cl]^+$	2.82×10^{-6}	−404	0.0053	4.07	
[c]$[Cu(5\text{-nitro-}1,10\text{-phen})_2Cl]^+$	1.65×10^{-6}	−389	0.0027	3.22	

[a] Obtained in DMSO + $TBAPF_6$ 0.1 M, Working electrode: Pt, scan rate = 0.1 V/s.
[b] pKa values taken from reference [64].
[c] Contribution of adsorption process.

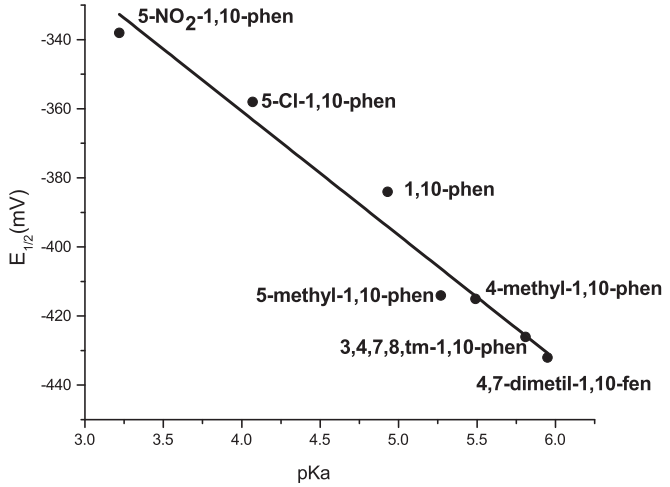

Fig. 8. $E_{1/2}$ (mV vs Fc-Fc^+) vs free ligand pKa correlation of the redox process $[Cu^{II}(N\text{-}N)_2NO_3]^+ + 1e \rightarrow [Cu^{I}(N\text{-}N)_2]^+ + NO_3^-$ in DMSO + 0.1 M $TBAPF_6$.

when different counterion (Cl^- or NO_3^-) is coordinated to the Cu(II) center and the different correlations obtained will be explained in the next section using DFT calculations.

Concerning to the apparent heterogeneous electron transfer constant (k_{app}) a correlation between this value and the π-acceptor character of the ligand is observed. Complexes with high π-acceptor character ligands, $[Cu(5\text{-}NO_2\text{-}1,10\text{-phen})_2NO_3]^+$ pKa = 3.22, show slightly higher values of k_{app} (0.0036 cm s^{-1}) in comparison with those complexes containing ligands with low π-acceptor, [Cu(3,4,7,8,tetramethyl-1,10-phen)$_2NO_3]^+$ pKa = 6.31 k_{app} = 0.0016 cm s^{-1}. This fact can be attributed to different reorganization energy for Cu(II) and Cu(I) oxidation states, due to backbonding effects. For chloro complexes no tendency between k_{app} and pKa is observed, probably due solvation effects control the electrode kinetics.

3.5. Theoretical calculations

To understand the distribution of the electronic density in the whole molecule Quantum Mechanics calculations were performed. Experimental and calculated distances are listed in Table 3. The difference observed in the electrochemical behavior could be associated to the distribution of the electron density obtained with the coordination of the chloride or the nitrate anions to metal center. As can be seen in Fig. 9, the frontier orbitals suffer a substantial modification with the change of coordinated anion. For the compound where chloride is coordinated to Cu(II), the HOMO orbital is localized principally in the latter, however when the nitrate anion is coordinated to the Cu(II), a dramatic change in the electronic distribution occurs and this orbital is located only in one of the coordinated phenanthroline. On the other hand, the LUMO orbital for the chloride derivative is located in both phenanthrolines meanwhile the LUMO orbital for the nitrate derivative is located in the opposite phenanthroline than that which holds the HOMO orbital.

It is clear from the Fig. 9, once the nitrate is coordinated to the copper ion; the electronic response of the compounds is controlled and modulated by the coordinated diimine. In this case, the electronic communication between the coordinated phenanthrolines mediated by the metal ion is strongly affected by the substituents on the phenanthroline moieties. (Fig. SI, Supplementary information). These facts could explain the linear relationship found between the diimine pKa and the redox potential of the coordination compounds in the case of the nitrate derivatives and the poor correlation when the chloride is in the coordination sphere of the metal ion.

3.6. Electrochemical study of $O_2^{\bullet -}$ in DMSO

Once it was demonstrated the modulation of half wave potential in Cu(II) complexes with diiminic ligands, the next step is study the electrochemical response of electro-generated superoxide. Fig. 10 show cyclic voltammograms of O_2 (2.1×10^{-3} M) in DMSO solution containing 0.1 M $TBABF_6$, where one reduction peak Ic and and two oxidation peaks Ia and IIa with potential peak values E_{pc}(Ic) = −1.318 V vs Fc-Fc^+, E_{pa}(Ia) = −1.046 V vs Fc-Fc^+ and E_{pa}(IIa) = 0.089 V vs Fc-Fc^+ were observed. Process I show a ΔEp = 0.272 V and a $E_{1/2}$ = −1.182 V vs Fc-Fc^+. According to the literature, corresponds to quasi-reversible electron transfer that generates the superoxide radical, $O_2 + 1e^- \rightarrow O_2^{\bullet -}$ [17]. Because of intrinsic moisture in the system, signal IIa may be associated with the direct oxidation of hydrogen peroxide, from the dismutation of $O_2^{\bullet -}$ to molecular oxygen, see the following scheme:

$$O_2 + 1e^- \rightarrow O_2^{\bullet -} \qquad \text{processIa}$$
$$2\,O_2^{\bullet -} + 2H_2O \rightarrow H_2O_2 + O_2$$
$$H_2O_2 \rightarrow O_2 + 2H^+ + 2e \qquad \text{process IIa}$$

3.7. Electrochemical study of $O_2^{\bullet -}$ in DMSO in the presence of H_2O

To determine the stability of $O_2^{\bullet -}$ in the presence of a proton donor, that can compete with copper complexes, experiments of oxygen reduction with different amounts water were carried out (Fig. 11). When the concentration of water was increased, a shift in potential peak values for signals Ia and IIa was observed. The first signal mentioned presented a decrease in current, and the second presented an increase.

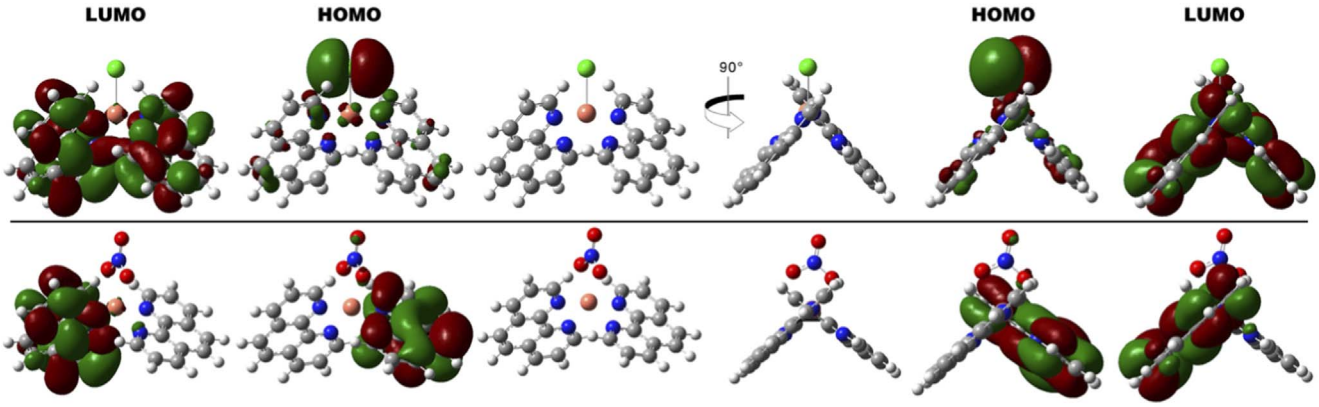

Fig. 9. Sketches for HOMO and LUMO orbitals of compounds $[Cu(1,10\text{-phenanthroline})_2Cl]^+$ (upper) and $[Cu(1,10\text{-phenanthroline})_2NO_3]^+$ (down) that show the modification in the orbitals distribution as a function of the metal's coordination sphere modification. The left side of the figure show one perspective of the orbitals; the right side show the same orbitals twisted 90° (isosurface value of 0.001).

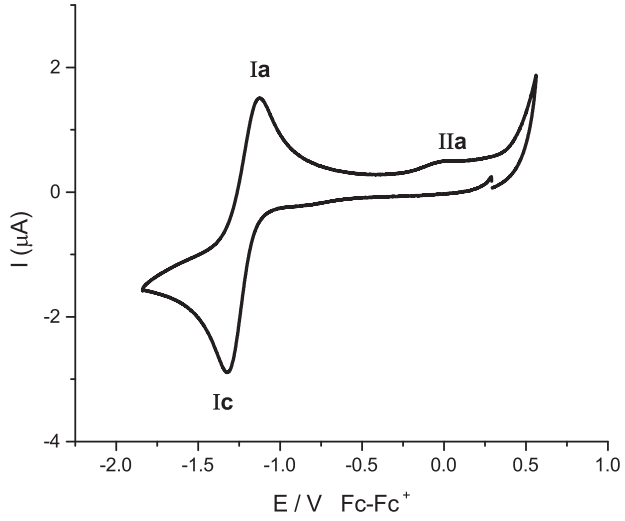

Fig. 10. Cyclic voltammogram of O_2 2.1 × 10^{-3} M in DMSO + $TBABF_6$ 0.1 M, cathodic direction. Working electrode: Pt. Scan rate = 0.1 V/s.

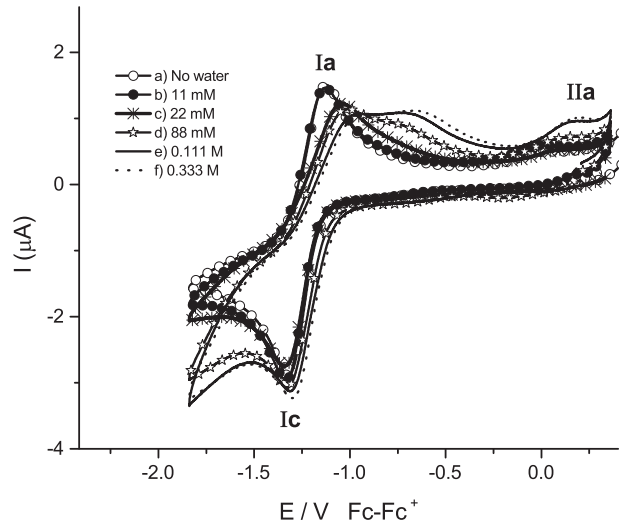

Fig. 11. Cyclic voltammogram of O_2 2.1 × 10^{-3} M in DMSO + $TBABF_6$ 0.1 M, cathodic direction in the presence of water in different concentrations. Working e lectrode: Pt. Scan rate = 0.1 V/s.

According to literature in process I, hydrogen bond associations between water and superoxide ion $O_2^{\bullet -}$ $(H_2O)_n$ with a typical formation constants, K_n^{ox} have been proposed [65–72]:

$$O_2 + 1e^- \rightarrow O_2^{\bullet -}(H_2O)_n \; K_n^{ox}, E_{1,n}{}^0, n = 1, 2$$

Additionally, changes in process IIa are related to an increase in the concentration of H_2O_2 coming from the reaction between $O_2^{\bullet -}$ and $2H_2O$, already mentioned.

3.8. Electrochemical reaction of metal complexes with superoxide anion

The reaction between the $[Cu(N\text{-}N)_2NO_3]^+$ and the radical $O_2^{\bullet -}$ was studied using cyclic voltammetry. Fig. 12 presents the electrochemical response of (a) the cationic complex $[Cu(3,4,7,8\text{-tm-}1,10\text{-fen})_2NO_3]^+$, (b) molecular O_2 and (c) the mixture of both components. As it was described in previous sections, the complex display the electrochemical reduction $[Cu^{II}(3,4,7,8\text{-}1,10\text{-phen})_2NO_3]^+ + 1e \rightarrow [Cu^{I}(3,4,7,8\text{-}1,10\text{-fen})_2]^+$ in process Ic, meanwhile the redox reaction from oxygen to superoxide is registered in process IIc, see Fig. 12b. In the experiment where the complex and O_2 are presented in DMSO solution, it is observed that signal Ic is not modified, contrary to what it is observed for signal IIc, where an increase in current is registered. In the case of oxidation signals Ia and IIa,

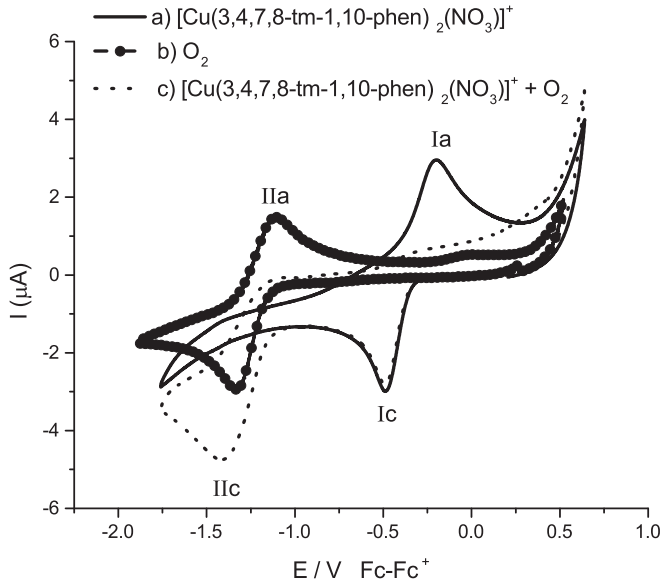

Fig. 12. Cyclic voltammograms of (a) complex $[Cu(3,4,7,8\text{-tetramethyl-}1,10\text{-phen})_2NO_3]^+$ 1 × 10^{-3} M, (b) O_2 2.1 × 10^{-3} M and (c) mixture of both in DMSO + $TBAPF_6$ 0.1 M, cathodic direction. Working electrode: Pt. Scan rate = 0.1 V/s.

these are not observed. It should be highlighted a remarkable difference in the electrochemical regeneration of oxygen from $O_2^{\bullet -}$, in comparison with experiments in the presence of water exclusively, indicating a high reactivity for metal complexes with superoxide.

The evidence allows us to propose an electrochemical disproportion (DISP) of $O_2^{\bullet -}$ by the $[Cu^{I}(3,4,7,8\text{-}1,10\text{-fen})_2]^+$ complex, however the competition with an ECE (Electrochemical-Chemical-Electrochemical) mechanism should not being discarded [73–74]:

$$[Cu^{II}(3,4,7,8\text{-tm}{-}1,10\text{-phen})_2NO_3]^+ + 1e \rightarrow [Cu^{I}(3,4,7,8\text{-tm-}1,10\text{-phen})_2]^+ + NO_3^-$$

$$O_2 + 1e^- \rightarrow O_2^{\bullet -}$$

$$2H^+ + [Cu^{I}(3,4,7,8\text{-tm-}1,10\text{-phen})_2]^+ \cdots O_2^{\bullet -} \rightarrow [Cu^{II}(3,4,7,8\text{-tm-}1,10\text{-phen})_2]^{2+} + H_2O_2$$

$$[Cu^{II}(3,4,7,8\text{-tm-}1,10\text{-phen}))_2]^+ + O_2^{\bullet -} \rightarrow [Cu^{I}(3,4,7,8\text{-tm-}1,10\text{-phen}))_2]^+ \ldots + O_2$$

$$2\,O_2^{\bullet -} + 2H + \rightarrow H_2O_2 + O_2$$

It is worth of mentioning the sum of stepwise proposed for process IIc results in an electrochemical disproportion (DISP) reaction already mentioned as $2\,O_2^{\bullet -} + 2H + \rightarrow H_2O_2 + O_2$ which is promoted by the metal complex. Therefore, we decided to calculate the ratio of the current of oxygen reduction (i_{O2CuL2}/i_{O2}) in presence and absence of metal complexes, as an indicator of the stability of $O_2^{\bullet -}$, and associated to a change in the mechanism from 1 to 2 electrons [73–74]. For $[Cu^{II}(3,4,7,8\text{-tetramethyl-}1,10\text{-phen})_2NO_3]^+$ 1.28 value is obtained. The same study was performed for all $[Cu^{II}(N\text{-}N)_2NO_3]^+$ complexes. Figs. 13 and 14 show the results for $[Cu(1,10\text{-phen})_2NO_3]^+$ and $[Cu(4,7\text{-dimetyl-}1,10\text{-phen})_2NO_3]^+$ complexes. The reaction at the electrode surface $[Cu^{II}(N\text{-}N)_2(X)]^+_{(ads)} + 1e^- \rightleftharpoons [Cu^{I}(N\text{-}N)_2]_{(ads)} + X^-$ interfere in the value of the ratio i_{O2CuL2}/i_{O2}. For this reason, complexes with Cl^- are not considered, in this analysis due the high adsorption process are observed. However, signals Ia and IIa, are not observed in the mixture of all complexes with oxygen. A summary of the values for all compounds studied in this work is presented in Table 4. Considering the redox potential of the Cu(II)/Cu(I) couple as descriptor of the ability to reduce the $O_2^{\bullet -}$ anion, the change in electrochemical reduction of O_2 measured trough the ratio (i_{O2CuL2}/i_{O2}) corresponding to an electrochemical disproportion mechanism (DISP), can be used as a numerical indicator of this process. As can be seen in Table 4, metal complexes with more negative redox potential, containing low π-acceptor ligands

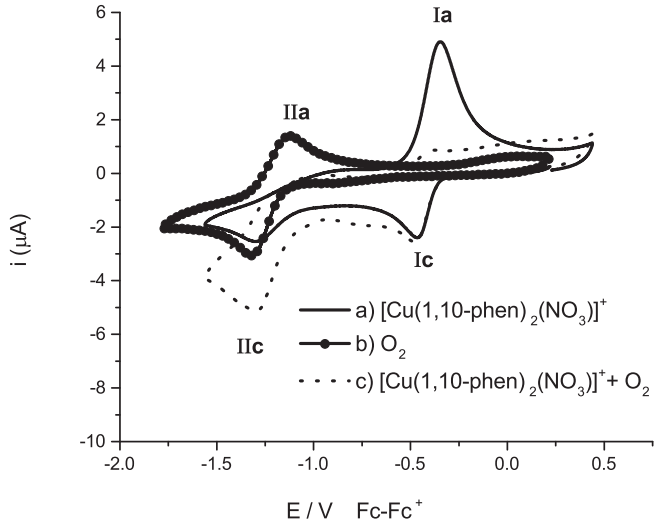

Fig. 13. Cyclic voltammograms of (a) complex $[Cu(1,10\text{-phen})_2NO_3]NO_3$ 1×10^{-3} M, (b) O_2 2.1×10^{-3} M y (c) mixture of both in DMSO + $TBABPF_6$ 0.1 M, cathodic direction. Working electrode: Pt. Scan rate = 0.1 V/s.

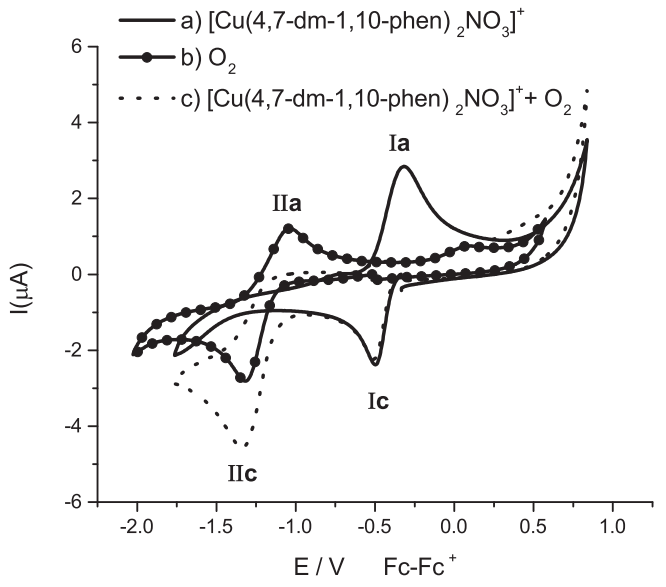

Fig. 14. Cyclic voltammograms of (a) complex $[Cu(4,7\text{-dimethyl-}1,10\text{-phen})_2NO_3]NO_3$ 1×10^{-3} M, (b) O_2 2.1×10^{-3} M and (c) mixture of both in DMSO + $TBAPF_6$ 0.1 M, cathodic direction. Working electrode: Pt. Scan rate = 0.1 V/s.

(high pKa), present a higher i_{O2CuL2}/i_{O2} ratio, than can be understood as a high capacity for $O_2^{\bullet -}$ disproportion. The results presented allow us establish the basis for a new simple method pointing to SOD-like mechanism, which can be used as a quick guide test before being proven in biological assays. However, in a future work metal complexes with a wide range of redox potential values and probe molecules in SOD assays such as, Nitroblue Tetrazolium (NBT) should be used to extrapolate the criterion established here for a biomimetic SOD compound. Other electrodes can be used to avoid adsorption processes.

4. Conclusions

The wave potential values ($E_{1/2}$) for electrochemical process $[Cu^{II}(N\text{-}N)_2(X)]^+ + 1e \rightarrow [Cu^{I}(N\text{-}N)_2]^+ + X^-$ showed a linear correlation with the free ligand pKa as a descriptor of π-acceptor character of the ligands. Complexes with redox potential more negative, favored the electrochemical disproportion mechanism (DISP) of superoxide ion, evidenced by the currents ratio (i_{O2CuL2}/i_{O2}) of process $O_2 + 1e \rightarrow O_2^{\bullet -}$ in the presence and absence of metal complex. Via electrochemical experiments, it was established a new methodology to SOD-like mechanism, which can be used as a quick guide test for any compound, before being proven in biological assays. This approach also indicates the capacity of a compound to react with superoxide.

Abbreviations

SOD	superoxide dismutase
1,10-phen	1,10-phenanthroline
DMSO	dimethyl sulfoxide
IR	infrared
FAB (+)	fast atom bombardment positive mode
ORTEP	Oak Ridge Thermal Elliptic Plot
DFT	density functional theory
UV–vis	ultraviolet visible
UV–vis-NIR	ultraviolet visible near infrared
ε	molar extinction coefficient
Λ	molar conductivity
$TBAPF_6$	tetrabutylammonium hexafluorophosphate
V	volts
V/s	volts/s
E_{pc}	cathodic peak potential
E_{pa}	anodic peak potential
$E_{1/2}$	$(E_{pa} + E_{pc})/2$, have wave potential
Fc/Fc^+	ferrocene/ferrocenium redox couple
ΔEp	$(E_{pa} - E_{pc})$, potential peak difference
HOMO	highest occupied molecular orbital
LUMO	lowest unoccupied molecular orbital
DISP	disproportion
ECE	electrochemical chemical electrochemical mechanism

Acknowledgement

The authors thank CONACyT (130500), UNAM-PAPIIT (217613) and UNAM-PAIP (3590-19) for financial support; and to CUVyTT (BUAP) for the facilities IR measurements; MEME, and MCR thank CONACyT and Red Temática Conacyt Farmoquímicos 280002. Authors also thanks M. Sc. Vladimir Carranza Téllez, Mass Spectrometry Laboratory, Centro de Química ICUAP, Benemérita Universidad Autónoma de Puebla (BUAP), for the acquisitions of Mass Spectra. `.

Appendix A. Supplementary data

Crystallographic data for this article have been deposited at the Cambridge Crystallographic Data Center as supplementary material number CCDC 1527171. Copies of the data can be obtained free of charge on application to CCDC, 12 Union Road, Cambridge CB2 1EZ, UK. E-mail: deposit@ccdc.cam.ac.uk. Supplementary information (SI) associated with this article can be found in the online version, at http://dx.doi.org/10.1016/j.jinorgbio.2017.07.013

References

[1] J.M. McCord, I. Fridovich, Free Radic. Biol. Med. 5 (1988) 363–369.
[2] I. Batinić-Haberle, J.S. Rebouças, I. Spasojević, Antioxid. Redox Signal. 13 (2010) 877–918.
[3] S.K. Dhar, D.K. St Clair, Free Radic. Biol. Med. 52 (2012) 2209–2222.
[4] G.R. Buettner, Anti Cancer Agents Med. Chem. 11 (2011) 341–346.
[5] G. Pani, R. Colavitti, B. Bedogni, S. Fusco, D. Ferraro, S. Borrello, T. Galeotti, Curr. Med. Chem. 11 (2004) 1299–1308.
[6] W.L. Oberley, R.G. Buettner, Cancer Res. 39 (1979) 1141–1149.
[7] M. Azad, M.O. Afzaal, P. Brien, Chem. Rev. 110 (2010) 4417–4446.
[8] B. Benyahia, F. Campana, B. Perderau, E. Gez, A. Fourquet, H. Magdelenat, Breast 5 (1996) 75–81.
[9] G. Vecchio, V. Lanza, J. Chem. Educ. 86 (2009) 1419–1421.

[10] V.J.A. Carceller, Universidad de Lleida,Tesis, (2007).
[11] N. Gerasimchuk, Z. Wang, J.L. Sessler, D.J. Magda, J. Am. Chem. Soc. (2005) 110–136.
[12] D. Salvemini, D.P. Riley, S. Cuzzocrea, Nat. Rev. Drug Discov. 1 (2002) 367–374.
[13] C.M. Cabello, W.B. Bair, G.T. Wondrak, Curr. Opin. Investig. Drugs 8 (2007) 1022–1037.
[14] C. Urquiola, D. Gambino, M. Cabrera, M.L. Lavaggi, H. Cerecetto, M. González, A.L. Cerain, A. Monge, A.J. Costa-Filho, M.H. Torre, J. Inorg. Biochem. 102 (2008) 119–126.
[15] K. Jitsukawa, M. Harata, H. Arii, H. Sakurai, H. Masuda, Inorg. Chim. Acta 324 (2001) 108–116.
[16] D.T. Sawyer, S. Valentine, J. Acc. Chem. Res. 14 (1981) 393–400.
[17] D.T. Sawyer, A.L. Sobkowiak, J. Roberts, Electrochemistry for Chemists, 2 (1995).
[18] H. Kuthan, H.J. Haussmann, J. Werringloer, Biochem. J. 237 (1986) 175–180.
[19] C. Beauchamp, I. Fridovich, Anal. Biochem. 44 (1971) 276–287.
[20] W.S. Szulbinski, P. Richard Warburton, D.H. Busch, Inorg. Chem. 32 (1993) 5368–5376.
[21] J.V. Mehta, S.B. Gajera, M.N. Patel, Spectrochim. Acta A Mol. Biomol. Spectrosc. 136 (2015) 1881–1892.
[22] M.A. Agotegaray, M. Dennehy, M.A. Boeris, M.A. Grela, R.A. Burrow, O.V. Quinzani, Polyhedron 34 (2012) 74–83.
[23] A.C. González-Baró, R. Pis-Diez, C.A. Franca, M.H. Torre, B.S. Parajón-Costa, B.S. Polyhedron 29 (2010) 959–968.
[24] B. Kripli, G. Baráth, É. Balogh-Hergovich, M. Giorgi, A.J. Simaan, L. Párkányi, J.S. Pap, J. Kaizer, G. Speier, Inorg. Chem. Commun. 14 (2011) 205–209.
[25] J.S. Pap, B. Kripli, V. Bányai, M. Giorgi, L. Korecz, T. Gajda, D. Árus, J. Kaizer, G. Speier, Inorg. Chim. Acta 376 (2011) 158–169.
[26] J.S. Pap, B. Kripli, T. Varadi, M. Giorgi, J. Kaizer, G. Speier, J. Inorg. Biochem. 105 (2011) 911–918.
[27] J.S. Pap, B. Kripli, I. Bors, D. Bogath, M. Giorgi, J. Kaizer, G. Speier, J. Inorg. Biochem. 177 (2012) 60–70.
[28] R.N. Patel, Y.P. Singh, Y. Singh, R.J. Butcher, Polyhedron 104 (2016) 116–126.
[29] R.N. Patel, D.K. Patel, V.P. Sondhiya, K.K. Shukla, Y. Singh, A. Kumar, Inorg. Chim. Acta 405 (2013) 209–217.
[30] Y.S. Hideki Ohtsu, A. Odani, O. Yamauchi, W. Mori, S. Itoh, S. Fukuzumi, J. Am. Chem. Soc. 122 (2000) 5733–5741.
[31] S.L. Dongfeng Li, D. Yang, J. Yu, J. Huang, Y. Li, W. Tang, Inorg. Chem. 42 (2003) 6071–6080.
[32] R.N. Patel, Inorg. Chim. Acta 363 (2010) 3838–3846.
[33] I. Spasojevic, R. Menzeleev, P.S. White, I. Fridovic, Inorg. Chem. 41 (2002) 5874–5881.
[34] A. Prisecaru, V. McKee, O. Howe, G. Rochford, M. McCann, J. Colleran, M. Pour, N. Barron, N. Gathergood, A. Kellett, J. Med. Chem. 56 (2013) 8599–8615.
[35] C. Li, B. Yin, Y. Kang, P. Liu, L. Chen, Y. Wang, J. Li, Inorg. Chem. 53 (2014) 13019–13030.
[36] Y.H. Zhou, J. Tao, Q.C. Lv, W.G. Jia, R.R. Yun, Y. Cheng, Inorg. Chim. Acta 426 (2015) 211–220.
[37] G. Csire, J. Demjén, S. Timári, K. Várnagy, Polyhedron 61 (2013) 202–212.
[38] S. Tabassum, S. Amir, F. Arjmand, C. Pettinari, F. Marchetti, N. Masciocchi, G. Lupidi, R. Pettinari, Eur. J. Med. Chem. 60 (2013) 216–232.
[39] P.C.J.L. Pierre, S. Refaif, C. Beguin, A.E. Marzouki, G. Serratrice, E. Saint-Aman, P. Rey, J. Am. Chem. Soc. 177 (1995) 1965–1973.
[40] Oxford Diffraction CrysAlis CCD; and CrysAlis RED, Oxford Difracction Ltd, England, 2009.
[41] R.C. Clark, J.S. Reid, Acta Crystallogr. A 51 (1995) 887–897.
[42] G.M. Sheldrick, Program for Crystal Structure Refinement, 2 University of Göttingen, Göttingen, Germany, 2008, p. 97.
[43] L.J. Farrugia, J. Appl. Crystallogr. 30 (1997) 565.
[44] L.J. Farrugia, J. Appl. Crystallogr. 32 (1999) 837–838.
[45] G. Gritzner, J. Kuta, Pure Appl. Chem. 56 (1984) 461–466.
[46] Y. Zhao, D.G. Truhlar, Theor. Chem. Accounts 120 (2007) 215–241.
[47] Y. Zhao, D.G. Truhlar, Acc. Chem. Res. 41 (2008) 157–167.
[48] R.F.W. Bader, Atoms in Molecules: A Quantum Theory (Oxford), (1990).
[49] P.L.A. Popelier, Atoms in Molecules: An Introduction, (2000).
[50] T.A. Keith, AIMAll (Version 13.11.04) (in), (2014).
[51] J.C. García-Ramos, R. Galindo-Murillo, A. Tovar-Tovar, A.L. Alonso-Saenz, V. Gómez-Vidales, M. Flores-Alamo, L. Ortiz-Frade, F. Cortés-Guzmán, R. Moreno-Esparza, A. Campero, L. Ruiz-Azuara, Chem. Eur. J. 20 (2014) 13730–13741.
[52] R. Galindo-Murillo, T.E. Cheatham III, Chem. Med. Chem. 9 (2014) 1252–1259.
[53] R. Galindo-Murillo, J. Hernandez-Lima, M. González-Rendón, F. Cortés-Guzmán, L. Ruíz-Azuara, R. Moreno-Esparza, Phys. Chem. Chem. Phys. 13 (2011) 14510–14515.
[54] M.J. Frisch, G.W. Trucks, H.B. Schlegel, G.E. Scuseria, M.A. Robb, J.R. Cheeseman, J.A. Montgomery, T. Vreven, K.N. Kudin, J.C. Burant, J.M. Millam, S.S. Iyengar, J. Tomasi, V. Barone, B. Mennucci, M. Cossi, G. Scalmani, N. Rega, G.A. Petersson, H. Nakatsuji, M. Hada, M. Ehara, K. Toyota, R. Fukuda, J. Hasegawa, M. Ishida, T. Nakajima, Y. Honda, O. Kitao, H. Nakai, M. Klene, X. Li, J.E. Knox, H.P. Hratchian, J.B. Cross, V. Bakken, C. Adamo, J. Jaramillo, R. Gomperts, R.E. Stratmann, O. Yazyev, A.J. Austin, R. Cammi, C. Pomelli, J.W. Ochterski, P.Y. Ayala, K. Morokuma, G.A. Voth, P. Salvador, J.J. Dannenberg, V.G. Zakrzewski, S. Dapprich, A.D. Daniels, M.C. Strain, O. Farkas, D.K. Malick, A.D. Rabuck, K. Raghavachari, J.B. Foresman, J.V. Ortiz, Q. Cui, A.G. Baboul, S. Clifford, J. Cioslowski, B.B. Stefanov, G. Liu, A. Liashenko, P. Piskorz, I. Komaromi, R.L. Martin, D.J. Fox, T. Keith, M.A. Al-Laham, C.Y. Peng, A. Nanayakkara, M. Challacombe, P.M.W. Gill, B. Johnson, W. Chen, M.W. Wong, C. Gonzalez, J.A. Pople, Gaussian Inc, (2009).
[55] N.F. Curtis, Y.M. Curtis, Inorg. Chem. 4 (1965) 804–809.
[56] K. Nakamoto, Infrared and Raman Spectra of Inorganic and Coordination Compounds: Part B: Applications in Coordination Organometallic and Bioinorganic Chemistry, 6th ed., 30-35 (1989), pp. 92–94.
[57] A.B.P. Lever, Inorganic Electronic Spectroscopy: 2a Ed, Elsevier, Amsterdam, 1984.
[58] S. Tyagi, B.J. Hathaway, J. Chem. Soc. Dalton Trans. 5 (1983) 199–203.
[59] L. Lu, S. Qin, P. Yang, M. Zhu, Acta Cryst E60 (2004) m574–m576.
[60] Y. Lei, F.C. Anson, Inorg. Chem. 33 (1994) 5003–5009.
[61] C.W. Lee, F.C. Anson, J. Am. Chem. Soc. 23 (1984) 837–844.
[62] R.S. Nicholson, Anal. Chem. 37 (1965) 1351–1355.
[63] A.J. Bard, L.R. Faulkner, Electrochemical Methods. Fundamentals and Applications, (2001).
[64] L. Gasque, G. Medina, L. Ruiz, R. Moreno, Inorg. Chim. Acta 288 (1999) 106–111.
[65] D.L. Maricle, W.G. Hodgson, Anal. Chem. 37 (1965) 1562–1565.
[66] C.P. Andrieux, P. Hapiot, J.M. Savéant, J. Am. Chem. Soc. 109 (1987) 3768–3775.
[67] C. Costentin, M. Robert, J.M. Savéant, J. Phys. Chem. C 111 (2007) 12877–12880.
[68] J.M. Savéant, J. Am. Chem. Soc. 109 (1987) 6788–6795.
[69] P.S. Singh, D.H. Evans, J. Phys. Chem. B 110 (2006) 637–644.
[70] C. Costentin, D.H. Evans, M. Robert, J.M. Savéant, P.S. Singh, J. Am. Chem. Soc. Comm. 127 (2005) 12490–12491.
[71] J.M. Savéant, J. Phys. Chem. C 111 (2007) 2819–2822.
[72] J.M. Savéant, Elements of Molecular and Biomolecular Electrochemistry, New Jersey. John Wiley & Sons, Inc., Hoboken, 2006.
[73] V.V. Smirnov, J.P. Roth, J. Am. Chem. Soc. 128 (2006) 3683–3695 (128).
[74] J. Serrano-Plana, M. Costas, M. Company, Inorg. Chem. 53 (2014) 12929–12938.